Available online at www.sciencedirect.com
ScienceDirect
Proceedings of the Combustion Institute 31 (2007) 3251–3259
Proceedings of the Combustion Institute
www.elsevier.com/locate/proci

From jet fuel to electric power using a mesoscale, efficient Stirling cycle

Alessandro Gomez [a,*], Jonathan J. Berry [b], Subir Roychoudhury [b], Bruno Coriton [a], James Huth [c]

[a] *Yale Center for Combustion Studies, Department of Mechanical Engineering, Yale University, P.O. Box 208286, New Haven, CT 06520-8286, USA*
[b] *Precision Combustion Inc., North Haven, CT, USA*
[c] *Sunpower, Inc., Athens, OH, USA*

Abstract

An approach to mesoscale electric power production is presented which relies on a clean and efficient combustor coupled with a free-piston Stirling engine. The design and development of a catalytic combustor is discussed, whose main components are: a multiplexed electrospray to disperse jet propulsion fuel (JP-8), a stack of catalytically coated grids through which fuel conversion and heat release is achieved cleanly and efficiently, and a recuperator to improve the system thermodynamic efficiency. The combustor/recuperator unit has a volume of 400 cm^3 and operates at a JP-8 flow rate on the order of tens of g/h, and equivalence ratios varying in the 0.35–0.70 range. The combustor is interfaced with a free-piston Stirling engine to achieve 42.5 W_e of power generation with a gross fuel–electric efficiency of 22%. With design optimization and the use of off-the-shelf auxiliary components (pump, blower, igniter, start-up battery, etc.), 21% efficiency *net* of parasitic losses is achievable in a unit with a volume of 2.61 and a mass of 1.7 kg (excluding fuel tank) and with a gravimetric energy density on the order of 1000–2000 W h/kg (3.6–7.2 MJ/kg), depending on fuel autonomy, that is, one order of magnitude larger than conventional batteries.

Keywords: Portable power; Mesoscale combustion; Electrospray; Catalytic; Free-piston Stirling engine

1. Introduction

Power generation is often the limiting factor in the miniaturization of portable equipment (e.g., mobile phones) and hampering further miniaturization. The situation is exacerbated as more and more functionality is added to such equipment. A critical parameter to compact power generation is gravimetric energy density, in terms of which fuels fare much better than conventional batteries. In fact, liquid hydrocarbons have a typical energy density of 42 MJ/kg to be compared to 0.6 MJ/kg of the ubiquitous Li-ion battery. Even operating with an overall fuel-to-electric conversion efficiency of 20%, fuel-based devices can in principle be more than one order of magnitude "denser" than conventional batteries, provided that their structures are sufficiently light. Moreover, they can be recharged easily and quickly, literally by refilling the tank.

* Corresponding author. Fax: +1 203 432 7654.
E-mail address: alessandro.gomez@yale.edu (A. Gomez).

1540-7489/$ - see front matter © 2006 The Combustion Institute. Published by Elsevier Inc. All rights reserved.
doi:10.1016/j.proci.2006.07.203

To harness the chemical power of fuels, small-scale combustion for thermal power generation enters the picture, as an intermediate step for subsequent conversion to electricity, as reviewed in [1]. Technological goals that have spurred researchers' interest in microcombustion include: micro-heat engines, as readily rechargeable batteries for electric power generation; microcombustors to power actuators in robotic applications; miniaturized internal combustion engines for the propulsion of micro air vehicles; and microthrusters to power small satellites. The power requirements of all these applications range between tens and a few hundreds of Watts, with the overall dimension of the device of several centimeters, despite invariably more optimistic projections. These dimensions, that are still small by conventional combustion standards, define what should be appropriately referred to as mesoscale combustion. At an even smaller overall scale is the concept of localized power generation for MEMS, to avoid "bussing around" electrical power. An example of future applications is powering "smart dust," that is, micro-sensors that monitor weather and air quality in a wireless network. This goal would require making thermochemical power sources sized at the microscale, with submillimeter feature size and overall dimensions of at most a few millimeters, so that every micro-device would carry its own power source to satisfy requirements on the order of perhaps only tens of mW.

Small-scale combustion presents fundamental limitations. As size decreases, the combustor surface-to-volume ratio increases. This, in turn, is a rough indicator of the ratio between heat loss and heat release rate. As a result, the system efficiency decreases and eventually combustion may not be sustainable. Moreover, even if steady combustion is established with an optimistic efficiency of energy conversion on the order of 20%, the majority of the fuel chemical energy is transformed to heat, proper management of which is crucial for the two following reasons. First, the dissipation of thermal energy is a major practical impediment in some applications, especially for certain consumer electronics and in military applications in which thermal signature is of primary concern. At a minimum, thermal management must intervene in the recuperation of the bulk of the energy contained in the exhaust to preheat the incoming reactant stream, under conditions of modest temperature differences across the combustor, as compared to conventional systems. In this way, the total reactant energy, including chemical and thermal components, can be higher than in the absence of recuperation, which has prompted the labeling of these systems as "excess enthalpy" burners [2]. Second, the efficient operation of an energy conversion system depends on maintaining a large temperature difference between the high temperature and the low temperature sides of some kind of thermodynamic cycle. Achieving this objective in a small volume is a major challenge. For that reason, microscale heat engines are inherently much more difficult to realize and, at best, a long prospect. At the mesoscale, on the other hand, the goal is within reach, as will be shown below.

We reported in the past on the successful demonstration of small-scale liquid fuel combustors using an electrospray for fuel dispersion and a catalytic reactor for fuel conversion [3,4]. We here address the adaptation of the combustor to a free-piston Stirling engine (FPSE) in the first successful demonstration of electric power generation from a notoriously problematic liquid fuel, JP-8, in an efficient mesoscale system.

2. Combustor design

A schematic of the system is shown in Fig. 1. Conceptually, the liquid fuel needs to be vaporized first, then mixed with the air and ultimately oxidized catalytically. Vaporization, mixing and oxidation are essentially in series and may all contribute to the overall combustor dimensions. However, our previous experience [3,4] suggests that the first two steps may play the controlling role. For the system to be highly efficient, a recuperator is needed to extract energy from the exhaust gases and preheat the oxidizer inlet gases.

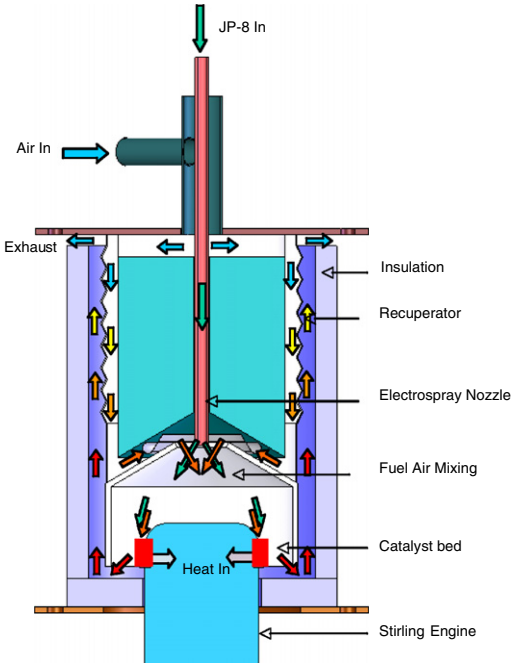

Fig. 1. Combustor and engine/interface schematic.

The energy released in the combustor is transferred to the FPSE through an optimized interface. Further details of the individual components follow.

2.1. Liquid fuel atomization

If the superior energy density of hydrocarbons with respect to batteries is to be exploited, the fuel has to be stored in the liquid phase. The simplest choice is to use highly volatile hydrocarbons such as propane or butane, that can be stored in the liquid phase and vaporize readily at room temperature. Heavier fuels, such as logistic fuels used in the military, need to be evaporated without being kept in contact with very hot surfaces to avoid fouling. Furthermore, the use of fuel blends such as JP-8 and the ensuing selective distillation may pose additional complications. As a result, liquid fuel dispersion by a suitable atomization technique seems better suited than a liquid film evaporator (e.g., [5]). A promising approach relies on the use of an electrospray (ES) to disperse the fuel in small, rapidly vaporizing droplets of uniform size, with negligible pressure drop [6]. The ES operates as follows: a conducting liquid emerging from the tip of a capillary tube is charged to a sufficiently high potential with respect to a ground electrode a short distance away, so that the liquid meniscus takes the shape of a cone from the tip of which a thin liquid thread emerges, in the so-called cone-jet mode [6]. This microjet breaks into a stream of charged droplets, which eventually spread to form the electrospray. Parasitic losses associated with the use of high voltage (kV) power supplies are minimal since the current drawn is on the order of 10 nA and the power drawn by the electrospray is a negligible fraction of the generated electric power, at $\ll 1\%$, even accounting for losses associated with voltage multiplication in high voltage power supplies.

As discussed in [6], the electrospray is characterized by a monotonic dependence of droplet diameter size on flow rate. Figure 2 shows the relation between droplet size (left ordinate) and liquid flow rate (abscissa), as measured by a fiber optic Phase Doppler System (TSI, Inc.) in experiments using a metal capillary operated in the needle/flat ground electrode configuration, similar to [6], with the system operating in the single cone-jet mode. In particular, for JP-8 doped with 0.05% on a mass basis of Stadis-450, to enhance its electric conductivity, the power law dependence is $D \propto \dot{Q}^{0.57}$. The size corresponding to the design flow rate of 14.5 g/h, which would yield 200 W of chemical power, is an unacceptably large 89 μm, as indicated by the dashed lines on the graph. To ensure fast evaporation and miniaturization of the mixing chamber preceding the combustion process, multiplexing the spray source by partitioning the total flow rate into a multitude of

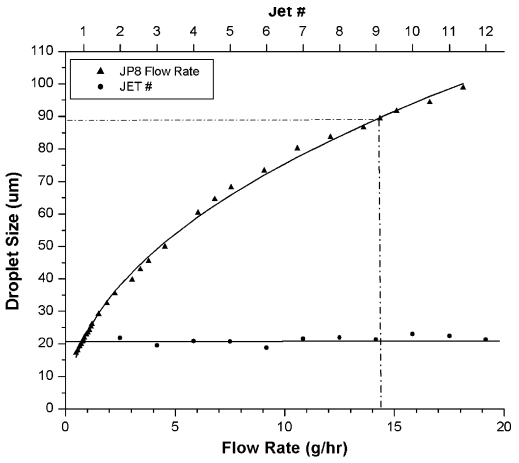

Fig. 2. Average droplet diameter in a cone-jet electrospray vs. JP-8 flow rate for a single cone-jet (lower abscissa) and number of each cone-jet anchored in the multi-jet mode to the grooved atomizer (upper abscissa).

jets operating in parallel is advantageous and should result in a reduction of the dimensions of the vaporization/mixing chamber, as compared to dispersing the fluid with a single electrospray.

To achieve this multiplexing, we relied on a novel approach to multiplexing based on a well-known, but hitherto unexploited, regime of operation, the multi-jet mode. At sufficiently high voltages a liquid that can be operated in the conventional cone-jet mode may disperse into a multitude of cone-jets emanating from a single bore and typically spreading out at an angle with respect to the axis of the nozzle through which the liquid is pumped [7]. Ordinarily, such a mode is rather unsteady and the range of flow rate at which appreciable multiplexing is achieved is small. However, the multi-jet mode may be stabilized as follows. The atomizer, a 3.2 mm O.D. stainless steel tube, was machined at the endface with 12 0.130 mm-wide grooves by wire-EDM. The objective of the grooves is to intensify the electric field at discrete points around its circumference, so that the cone-jets are simultaneously anchored at these features. Figure 3 shows the electric field along an arc of the circumference of a sample atomizer, as obtained by postprocessing the solution of the Laplace equation for the electric potential using FEMLab [8] for a simplified nozzle geometry with only four grooves, to minimize the computational time with the desired spatial resolution. The field, computed at the outermost radial location, revealed the presence of spikes, corresponding to the location of the grooves, where the field intensity is at least a factor of two larger than the background value along the rest of the circumference. Since no account was taken of the presence of the liquid that was wetting the surface nor of the charged droplets

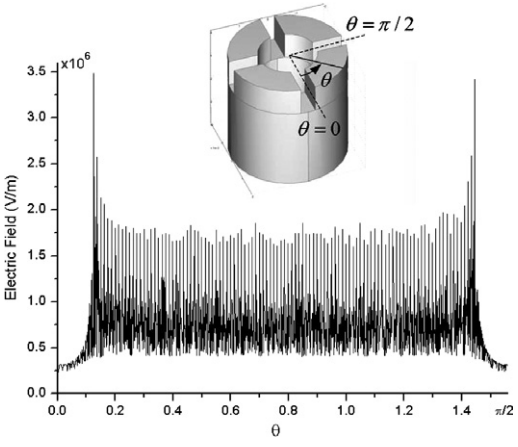

Fig. 3. Electric field computed as a function of the polar coordinate, θ, around the tube quarter circumference.

and attending space charge, the results are to be considered qualitative. Nevertheless, they are revealing since they show a periodic electric field along the circumference of the nozzle, with peaks in correspondence of the grooves that are much larger than the background field at the nozzle.

As a result of this modification, a stable mode of operation is identified over several hundreds of volts and a broad range of flow rates. Figure 2 shows the average droplet size in each electrospray in the multi-jet mode anchored around the grooved atomizer of Fig. 3, as identified by a number in the right ordinate. Most importantly, so long as the machining is precise, as is the case with wire EDM, the average droplet in each electrospray does not vary significantly in size from spray to spray, as shown in Fig. 2, which suggests that the total flow rate is equipartitioned among the sprays. To quantify the size scatter from jet to jet, a relative standard deviation (RSD) is defined as

$$\mathrm{RSD} = \frac{1}{\bar{D}}\sqrt{\sum_{i=1}^{N}(\bar{D}_i - \bar{D})^2/(n-1)},$$

where $\bar{D}_i$ is the average droplet diameter for jet i, and $\bar{D} = \sum \bar{D}_i/n \cong 21.1\ \mu\mathrm{m}$ is the droplet size averaged over all jets. The uniformity of the droplet size is good, with the RSD ~ 0.06, which is comparable to the degree of non-uniformity in size within a single jet. This size uniformity is important since the length of the evaporation chamber in the streamwise direction is affected by the slowly evaporating, largest droplets in the distribution. Such a role cannot be downplayed since large droplets contain a high fraction of the total liquid volume. Figure 2 shows that, if the total JP-8 flow rate is partitioned in 12 electrosprays, the droplet size at the injection is reduced by a factor $(1/12)^{0.57} = 4.1$. A further reduction can be achieved by increasing the voltage within the stable multi-jet mode. Since the droplet evaporation time scales with the square of the droplet diameter, the evaporation time would be reduced by a factor of 17. An estimate of the evaporation coefficient for JP-8 at the prevailing average temperature of 1000 K yields a value of 0.3 mm^2/s [9], which results in a characteristic time for evaporation on the order of 1.5 ms. At the volumetric flow rate of approximately 250 cm^3/s at an average combustor temperature of 1000 K, the average residence time in the mixing/evaporation chamber volume of 6.6 cm^3 is 2.7 ms, which guarantees that at steady state by the time the mixture reaches the catalyst reactor evaporation has been completed, even accounting for the droplet flight time across the chamber. Further details on the atomizer behavior are given in [10].

2.2. Fuel/air mixing and ignition

To minimize the volume of the mixing chamber preceding catalytic conversion of fuel into combustion products, an option is to use a whirling flow field by introducing air with a tangential velocity component into the cylindrical chamber [11]. The effect of air whirl was evidenced in [4] by comparing whirl injection with coaxial air injection from the burner bottom and showing that the first markedly improved temperature uniformity on the catalytic surface, which is crucial for efficient coupling with a Stirling engine. In fact, uniformity of temperature relates directly to the homogeneity of the local equivalence ratio. To that end, a low pressure drop radial swirler was coaxially located with the fuel nozzle a few millimeters downstream of the atomizer (Fig. 1). It resulted in uniform mixing of the recuperated inlet air and the fuel droplets. A resistively heated element, via an arrangement analogous to a glow plug, was used to heat the catalyst and light it off, in the presence of fuel and air, at ambient conditions. Power from an onboard rechargeable battery was used to energize the igniter.

2.3. Catalytic combustion

The increase of the surface-to-volume ratio with miniaturization favors the catalytic approach especially at the small scale, where surface effects are very significant. This approach was implemented in the combustor by incorporating a compact reactor design based on the use of a series of catalyst coated metal grids (Microlith®, Precision Combustion, Inc. (PCI), North Haven, CT, USA) [3,4]. The grids were stacked serially, each with short channel lengths, high cell density and low thermal mass. The resulting reactor was very compact, had rapid transient response and high energy

density, and required small amounts of precious metal catalysts. Catalyst formulations were selected from platinum group metals and an alumina washcoat with appropriate additives. The advantages of this design stem from the reduction in mass transfer limitations, as compared to conventional monoliths having relatively thick boundary layers. Also, under conditions of chemical kinetic control, the particular design can pack more active area into a small volume, which means that insertion of such catalysts in a flow can provide more effective fuel conversion for a given pressure drop. The catalytic reactor discussed in [4,5] had a planar configuration. The use of thin and flexible microliths made the conformation to specific geometric requirements relatively easy. In particular, since the hot end of the Stirling engine (Fig. 1) is a cylindrical strip, the reactor was cylindrically shaped by placing the microlith catalytic grids around the acceptor zone of the FPSE and flowing the air-fuel mixture through it. The average residence time across the catalytic reactor was estimated at ~0.8 ms, which, as expected, is much smaller than the estimated evaporative and mixing time. The prevailing Peclet number was estimated at 30, which required the stacking of several layers to complete fuel oxidation [12]. From durability tests [4], it is anticipated that periodic maintenance of the energy converter will require catalyst replacements at intervals on the order of 1000 h. Despite the mesoscale of the combustor and the potential for high losses, a respectable 30 MW/m^3 of volumetric power density was achieved in the total volume of the evaporation/mixing chamber and the catalytic reactor.

2.4. Exhaust gas recuperation

The exhaust gas was rerouted through a counterflow heat exchanger consisting of a corrugated metal lamina separating the exhaust from the incoming air, while allowing for heat transfer between the two gases. As sketched in Fig. 1, the recuperator occupied a cylindrical jacket wrapping the burner. This geometric configuration was also chosen to avoid preheating the fuel line because of the fouling risk associated with the use of jet fuel. Temperature measurements via K-type thermocouples, at the inlet and outlet of the recuperator, yielded an estimated heat recovery effectiveness of 85% and an inlet fresh air temperature of 980 K. In addition to boosting the overall thermal efficiency of the combustor, the recuperator has the important function of reducing the droplet evaporation time by elevating the average temperature in the combustor to 1000 K, thereby increasing the evaporation coefficient several folds. The exhaust gas temperature at 450 K can be further decreased by mixing it with the engine cooling air at 350 K, to lower the system thermal signature.

3. Free-piston Stirling engine (FPSE)

The Stirling cycle has been a favorite of thermodynamicists because of its high thermodynamic efficiency. Its practical appeal is that it is an external combustion engine, whose operation does not depend on the type of fuel used to provide heat. An ideal Stirling cycle with regeneration can approach 55–60% Carnot efficiency, which is still much better than other heat engines. Its linear free-piston realization is distinct from the kinematic Stirling with its disadvantages of life-limiting seals and bearings, the need for lubrication, and the difficult control of the power output. The free-piston Stirling engine replaces the complex crank mechanism of the kinematic machine with a linear alternator connected directly to the piston. The engine is hermetically sealed, quiet, with low vibration, contains gas bearings for non-contact operation of moving components, requires no lubrication, has long life and provides direct AC output. The 35 W_e (EE-35) FPSE design used in the present application has been developed by Sunpower, Inc. (Athens, OH, USA). It has a thermal-to-mechanical conversion typically near 35% and a thermal-to-electrical conversion near 32%. Specific to the present system were efforts to minimize the engine controls and integrate them with those of the combustor.

4. Combustor/engine interface

Under full load conditions, the average catalyst temperature over multiple runs was 1002 K and an average FPSE head temperature of 923 K. With these values, one can estimate the dominant heat transfer between the catalytic reactor and the engine head. To increase the heat transfer between the two system components a finned cylinder was brazed onto the engine head. The catalyst was placed in conductive contact with the engine head. Thermocouple measurements in the catalyst bed and at the exit of the fins suggested that the convective heat recovery from the fins was on the order of 10 W. The balance to the thermal input into the engine of ~133 W_t cylinder was met conductively, as confirmed by estimates based on the interface geometry and an average thermal conductivity for Nickel 201 over the temperature range under consideration of 62.9 W/mK. The balance of the 200 W_t input as chemical energy was split into a loss of 30 W_t associated with the exhaust gases at 450 K after recuperation, and 38 W_t of various other losses associated with imperfect insulation of the structure. Note that the heat transfer efficiency from the fuel to the head was compromised due to heat losses, e.g., flanges and thick walled chambers acting as heat sinks in the test setup, radiative and convective losses to the exhaust, limited

insulation, etc. Once optimized, it is likely to improve the overall fuel-to-electric efficiency.

5. Fuel-to-electric efficiency

The schematic in Fig. 4 shows the system key components with individual efficiencies/effectivenesses. From the efficiency of the individual components, a burner efficiency can be defined as the ratio of the thermal power input to engine over the chemical power associate with the mass flow rate of a fuel of a prescribed heating values, that is,

$$\eta_{\text{Burner}} = \frac{\dot{Q}_{\text{toengine}}}{\dot{Q}_{\text{fuel}}} = \eta_{T-\text{Loss}} \frac{\eta_{\text{Interface}}}{1-\eta_{\text{Recuperator}}(1-\eta_{\text{Interface}})},$$

whose functional form reflects the fact that some of the components are in parallel. An overall fuel–electric efficiency can be defined a by multiplying it by the engine efficiency, that is, $\eta_{\text{ov}} = \eta_{\text{Burner}}\eta_{\text{FPSE}}$ (electrical power out/fuel chemical power). The burner efficiency, η_{Burner} at full load was ≈70%. The gross system efficiency, η_{ov}, was measured at 22%, excluding parasitic losses from auxiliary components.

A general characteristic of a FPSE is that its power output is roughly proportional to the square of the engine piston amplitude [13]. Figure 5 shows this dependence and that of the engine efficiency versus piston amplitude [14]. The control approach consists in varying the piston amplitude via a controller to match engine power output to the external load demand. The burner firing rate is then varied to maintain a constant FPSE acceptor temperature, regardless of the amount of heat being accepted by the engine. As shown in Fig. 5, the heat input-to-electrical output conversion efficiency of the Sunpower 35 W_e (EE-35) engine is fairly constant over a wide range of piston amplitude. As a result, the efficiency of the FPSE will remain constant over a wide range

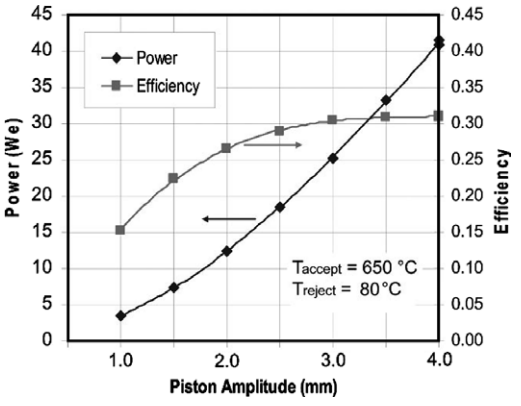

Fig. 5. Power and efficiency (ratio of electrical output to heat input) versus piston amplitude for the Sunpower 35 W_e (EE-35) FPSE.

of system output power. Additionally, a test was done to explore part load efficiencies by reducing the head and burner operating temperatures (Fig. 6). The burner was operated at full load and the head temperature was allowed to vary with JP-8 flow while the engine displacer and piston stroke amplitudes were held nearly constant. The reduced burner operating temperature also reduced heat losses as well as recuperator losses. This test demonstrated improved efficiency for part load operation under "constant displacement" conditions. A 2% higher gross efficiency over "constant head temperature" operation at 54% load was observed. This data also indicated that the output power could be effectively controlled by the fuel flow rate.

Remarkably, even though the fuel source is the notoriously problematic JP-8, with attending coking and sooting tendency, the burner operated cleanly for several hours (~50 h) with no noticeable traces of deposits. JP-8 contains high levels of sulfur that are known coke precursors. The catalytic mesh however minimizes boundary layer buildup and results in remarkably high heat and mass transfer coefficients. This, in conjunction

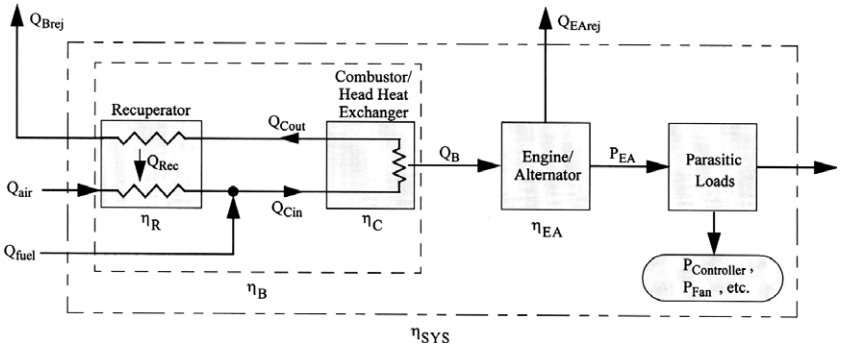

Fig. 4. Schematic of the system components and energy flow.

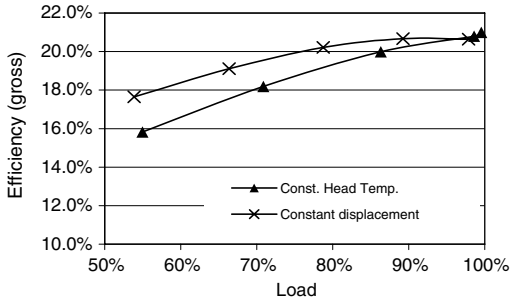

Fig. 6. System efficiency vs. load under conditions of either constant engine head temperature or constant displacement.

with the high surface area, augments diffusion, mixing, and oxygen transport to the surface, and permits practically complete conversion of the fuel, reducing the tendency to coke. The power consumption of off-the-shelf auxiliary components, based on commercially available devices, yields an overall efficiency of 18% net of parasitic losses. Table 1 shows some figures of merit of the power convertor, inclusive of realistic projections on total weight, volume, energy density, once the system is integrated in a stand-alone device from the current breadboard version. Figure 7 shows a picture of the first generation integrated system. Currently, the only component yet to be completed for this stand-alone device is the engine controller. The resulting unit will have an energy density in the range 3.6–7.2 MJ/kg, depending on fuel autonomy, that is dramatically better than a conventional Li-ion battery at 0.6 MJ/kg. Excluding fuel tank, the unit is expected to weigh 1.7 kg in a volume of 2.61.

If one compares the measured efficiencies with those of portable power generators in the kW range, the efficiency of 18% obtained in the present system is particularly significant, since the system is much smaller, which should have resulted in greater losses because of the higher surface-to-volume ratio.

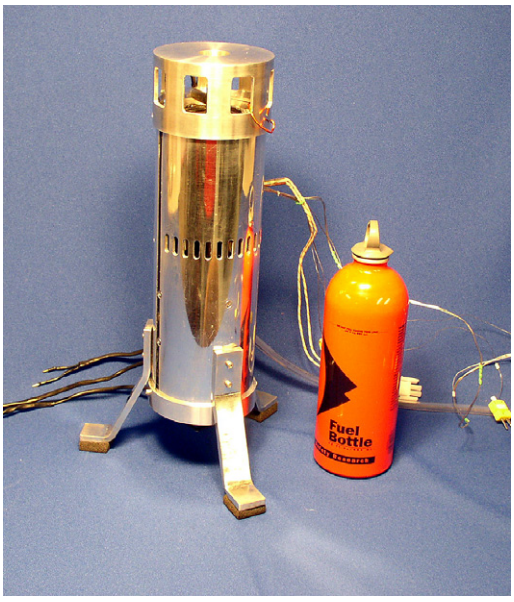

Fig. 7. Picture of the first generation integrated system with separate fuel tank.

6. Conclusions

The integration of a JP-8 catalytic combustor with a free-piston Stirling engine was demonstrated. The burner consisted of: a fuel dispersion system based on the electrospray; a catalytic reactor using a stack of coated meshes for complete fuel conversion; a carefully designed engine interface to optimize the heat transfer into the engine; a recuperator to recover some of the thermal energy

Table 1
System figures of merit

	Current status	Projected performance
Overall burner efficiency, η_{burner}	70%	78%
Gross JP-8 to electric efficiency, η_{ov} (gross)	22%	25%
Net JP-8 to electric efficiency, η_{ov} (net)	18%	21%
Isolated engine/alternator output power	42.5 W_e	42.5 W_e
Parasitic loads	8 W_e	7.5 W_e
Net system output power	34.5	35 W_e
Isolated engine/alternator efficiency	32%	32%
Engine/alternator mass	656 g	440 g
Combustor mass	311 g	311 g
System mass (dry, includes all components)	2100	1700 g
Fuel	JP-8	JP-8
Maximum T (hot end)	650 °C	650 °C
Maximum T (cold end)	70 °C	70 °C
System volume	2.7 l	2.6 l
System specific power, (dry)	16.4 W/kg	21.1 W/kg
System specific energy, (wet, 3 days operation)	800 W h/kg	943 W h/kg
System specific energy, (wet, 10 days operation)	1505 W h/kg	1668 W h/kg

from the exhaust and increase the system thermodynamic efficiency; and the 35 W_e Sunpower Stirling engine. The combustor/recuperator has a volume of 0.4 l and operates at JP-8 flow rates on the order of tens of g/h, and equivalence ratios varying in the 0.35–0.70 range. No soot or coke deposits were found after several hours of operation. Preliminary results with a breadboard unit showed a gross fuel–electric efficiency of 22% (18% net of parasitic). Feasible design optimization should yield 21% efficiency *net* of parasitic losses, with an energy density on the order of 1000–2000 W h/kg (3.6–7.2 MJ/kg), depending on fuel autonomy, in a unit weighing 1.7 kg with a volume of 2.6 l (excluding fuel). These figures are significantly better than even larger commercially available generator sets.

Acknowledgments

We acknowledge the help of Messrs. Weiwei Deng (Yale), for performing the field calculations of Fig. 3, and N. Bernardo (Yale) for machining some of the hardware. The support of DARPA, under Grant No. DAAD19-01-1-0664 (administered by ARO, Dr. Richard J. Paur, Contract Monitor), is gratefully acknowledged. Microlith® is a trademark of Precision Combustion Inc.

References

[1] A.C. Fernandez-Pello, *Proc. Combust. Inst.* 29 (2002) 883–889.
[2] S.A. Lloyd, F.A. Weinberg, *Nature* 257 (1975) 367–370.
[3] D.C. Kyritsis, I. Guerrero-Arias, S. Roychoudhury, A. Gomez, *Proc. Combust. Inst.* 29 (2002) 965–972.
[4] D.C. Kyritsis, B. Coriton, F. Faure, S. Roychoudhury, A. Gomez, *Combust. Flame* 139 (2004) 77–89.
[5] W.A. Sirignano, T.K. Pham, D. Dunn-Rankin, *Proc. Combust. Inst.* 29 (2002) 925–933.
[6] K. Tang, A. Gomez, *Phys. Fluids A* 6 (1994) 2317.
[7] M. Cloupeau, B. Prunet-Foch, *J. Electrostat.* 25 (1990) 165–184.
[8] COMSOL, Inc., <http://www.comsol.com/>, 2005.
[9] A.H. Lefebvre, *Atomization and Sprays*, Taylor and Francis, New York, 1989.
[10] M.H. Duby, W. Deng, K. Kim, T. Gomez, A. Gomez, *J. Aerosol. Sci.* 37 (2006) 306–322.
[11] R.A. Yetter, I. Glassman, I.H.C. Gable, *Proc. Combust. Inst.* 28 (2000) 1265–1272.
[12] M. Vera, A. Liñán, *Combust. Theory Model.* 8 (2004) 97–121.
[13] I. Urieli, D. Berchowitz, *Stirling Cycle Engine Analysis*, Adam Hilger, Ltd., Bristol, UK, 1984.
[14] S. Kim, J. Huth, J. Wood, AIAA-2005-5540, 3rd International Energy Conversion Engineering Conference, San Francisco, California, Aug. 15–18, 2005.

Comments

Derek Dunn-Rankin, University of California Irvine, USA. The specific energy (or energy density) depends on operating duration since maximum specific energy occurs when the mass of the fuel carried is much larger than the mass of the chemical–electrical energy conversion system. In this case, as you indicate, the conversion efficiency is the important figure-of-merit. For shorter missions, however, other trade-offs may become critical. In this context, please comment on the electrospray-Stirling system specific energy performance as a function of mission duration.

Reply. Indeed, mission duration is a very important variable. The energy conversion system we developed is well-suited for missions of duration ranging from a few to several days. Table 1 reports the current energy density at 800 and 1505 W-h/kg, for fuel autonomy of 3 days and 10 days, respectively. The goal of achieving energy densities one order of magnitude larger than Li-ion batteries is clearly reached.

•

Carlos Fernandez-Pello, University of California Beckely, USA. When comparing different power systems it is important to compare those with similar power density or size. At small scale, particularly near limiting conditions, the efficiency of the device is strongly dependent on size, thus it is not correct to compare efficiencies of systems that have different sizes. For example, our rotary engine, currently providing 30 W with 4% efficiency, would provide several times the power and have much higher efficiency if its size would be doubled.

Reply. Indeed, the challenge of achieving large energy density and high efficiency becomes more difficult to meet the smaller is the system, as discussed at the end of Section 5 in the article. That is the reason why achieving the present energy densities, at the efficiencies reported and, most importantly, using a liquid fuel like JP-8, required much development work. We will be very interested in learning details about the performance of the Berkeley rotary engine once it is documented in the peer-reviewed literature.

•

Dimitrios Kyritsis, University Illinois Urbana-Champaign, USA. Do you expect losses due to air pumping in a practical device?

Why is the catalytic reactor limited in the annulus you showed and does not cover the entire Stirling engine head?

Reply. Air pumping losses associated with the pumping of the oxidizer in the combustor and the cooling requirements of the Stirling engine are estimated at <1 W(electrical), that is ~2% of the total electric power generated.

The engine acceptor is only the specified annulus. The engine dome is not supposed to be heated, except for inevitable heat conduction effects, because of the specific design of the Stirling engine.